OE Optical Engineering

RESEARCH PAPER

Measurement-based characterization of atmospheric background light in satellite-to-ground quantum key distribution scenarios

Stefanie Häusler,* Davide Orsucci, Leonard Vollmann, Eltimir Peev, and Florian Moll

Institute of Communications and Navigation, Optical Satellite Links, German Aerospace Center, Wessling, Germany

ABSTRACT. Quantum key distribution (QKD) enables private communication with information theoretic security. Free-space optical communication allows one to implement QKD without the limitations imposed by fiber networks such as the exponential scaling of transmission losses in optical fibers. Therefore, free-space QKD via satellite links is a promising technology to provide long-distance quantum communication connections. In free-space QKD systems, background light is the main source of noise, which has to be suppressed by means of spectral, spatial, and temporal filtering to reach a sufficiently low quantum bit error rate (QBER). Only then a quantum key can be exchanged successfully. To be able to define the requirements for a free-space QKD system, the background light must be examined more closely. Current considerations concentrate on cloud-free skies and rural environments. Free-space QKD will also take place when the sky is partly clouded and most likely also in urban environments. Here, an overview of physical causes of background light for downlink scenarios is given. Furthermore, the relation between QBER and background light is derived for a decoy-state BB84 protocol with polarization-encoded qubits to give an example of the dependency. Moreover, a setup to experimentally investigate the background light is shown. Measurement data were taken with this setup in Oberpfaffenhofen near Munich (Germany) in C-band. The measurement data are used to verify a background light simulation tool. The outcome underlines that simulation tools are sufficient for clear sky scenarios.

 [DOI: 10.1117/1.OE.63.4.041211]

Keywords: quantum key distribution; background light; quantum key distribution receiver; quantum bit error rate; optical ground station

Paper 20230871SS received Sep. 29, 2023; revised Dec. 21, 2023; accepted Dec. 27, 2023; published Feb. 6, 2024.

1 Introduction

The security of today's cryptographic methods is threatened by advancing research on quantum computers, as these quantum computers may solve mathematical problems on which current public-key encryption methods are based. Quantum key distribution (QKD) is emerging as a promising method that is able to guarantee long-term and future-proof secure communication. In principle, fiber connections can be used to distribute the quantum key. Free-space ground-to-ground links can bridge broken or nonexisting fiber connections when line-of-sight is given. Enabling QKD over long distances is a challenge when using fibers since optical fibers have

*Address all correspondence to Stefanie Häusler, stefanie.haeusler@dlr.de

0091-3286/2024/$28.00

an exponential loss with distance. Therefore, one concept to overcome this limitation is to distribute the key via a mobile node such as a satellite, an aircraft, or a high-altitude pseudo-satellite. One advantage of this scheme is that atmospheric extinction losses can be neglected beyond a height of around 10 km as the density of the atmosphere decreases rapidly with an increase of altitude.[1]

The feasibility of free-space QKD is dependent on the signal-to-noise ratio (SNR). In classical communications, the SNR can be improved by increasing the signal and decreasing the noise level. In QKD, the SNR is even more crucial because the transmitted signal ideally consists of one photon or, in practice, a weak coherent pulse with very low mean photon number. Therefore, one cannot increase the transmitted signal power to increase the SNR. The noise has contributions both from the intrinsic noise of the instruments as well as extrinsic ambient noise, which is the background light. Noise will cause an increase in the quantum bit error rate (QBER). At a given threshold of the QBER, the key distributed has to be aborted because it is no longer possible to upper-bound the amount of information accessible to a potential eavesdropper. This threshold is different for different scenarios and protocols.[2]

Several publications state the importance of background light and some also provide approaches for dealing with background light to make free-space QKD scenarios feasible. The power of diffuse background light coupled into the free-space detector depends on brightness of the sky background, field of view (FOV) of the receiver telescope, receiving telescope aperture, and absolute bandwidth of the filter in front of a detector.[1,3,4] The brightness of the sky can be calculated using simulation software such as library for radiative transfer (LibRadtran) or MODerate resolution atmospheric TRANsmission (MODTRAN).[2,3,5] The outcome of this software is evaluated by a brightness measurement carried out over one day from 9 am to 5 pm at different zenith angles in previous work.[5] A model for daytime sky access for satellite QKD downlinks is presented. The output of this model is a hemispherical color density map of the QBER for different optical setups and different time of the year.[2] These models help to define the requirements to reduce background light to enable QKD during daylight and in urban environments. Methods of noise suppression are spectral filtering and temporal filtering. Furthermore, spatial filtering can be applied. Using adaptive optic, the spot size of the quantum signal is decreased and therefore a smaller field stop in front of the detector can be applied to reduce noise.[5]

These models analyze the background light during day and night at different locations assuming the ideal condition of a cloud-free sky in a rural environment. Therefore, they allow one to define rough requirements for QKD systems under consideration of the assumptions. The question arises whether it is sufficient to estimate the background light with the assumption of an ideal environment or not. If there are large variances between existing simulations and actual measurable values, satellites and ground stations would have to be modified after development. This can be prevented by analyzing this issue in detail by experimental means and incorporating the results into the design of satellites and ground stations of the future.

To become aware of all existing sources of background that affect the system, these are outlined in Sec. 2. Furthermore, the calculation of the propagation of light through the atmosphere is explained in Sec. 2. The calculation of the dependence between QBER and background light is shown on the decoy-state BB84 protocol for polarization-encoded qubits in Sec. 3. The importance of the influence of the background light is discussed on the basis of this derivation. Simulation results will be evaluated by experimentally determined background light. The principle of the experiment is explained in Sec. 4. Measurements were taken during a free-space QKD experiment in an urban environment and a clear sky brightness scan was performed. These measurement results are presented in Sec. 5. In Sec. 6, the measurement results are compared with the results of the simulation and the question is addressed whether existing simulation tools are sufficient. Finally, Sec. 7 gives a conclusion and an outlook for further research in this field.

2 Sources of Background Light and Propagation Through the Atmosphere

To characterize the amount of background light arriving at the detector, one has to be aware of the different sources that cause background light. These sources are summarized in Table 1.

Table 1 Sources of diffuse and direct background light in free-space QKD systems.

Sources of background light	Impact
Solar sky radiance	Diffuse
Lunar sky radiance	Direct and diffuse
Stars and planets	Direct and diffuse
Zodiacal light, airglow, and diffuse emission in the galaxy	Diffuse
Reflections on surface of transmitter device	Direct
Channel crosstalk	Direct and diffuse
Anthropogenic light	Diffuse

The source's impact can be diffuse or direct. Both increase noise whereas direct radiation may even disturb sub-systems, which are needed for the operation of the link, such as the tracking, and may also lead to a rather rapid noise increase when the telescope's FOV moves towards the source's direction. As the C-band is investigated here, thermal radiation emitted by the atmosphere can be neglected since the temperature is too low.[6] The main source of radiation incident on Earth is the Sun. At 1550 nm, the solar spectral irradiance above the atmosphere is 270 $\mathrm{mW/m^2nm}$.[7] This value varies throughout the year as the Sun-to-Earth distance changes. Only the diffuse part of the Sun's radiation is of importance for optical communication because the Sun is generally avoided by telescopes. At night, multiple sources such as the Moon, stars, and planets need to be taken into account. As the telescope is not avoiding the direct impact zone of these, the direct and diffuse radiation needs to be taken into account here. There are also diffuse sources in the night sky, namely zodiacal light and airglow, as well as diffuse emissions from within the galaxy. Furthermore, light can be scattered off the environment in which the QKD transmitter is placed, e.g., the satellite or a building structure. Moreover, channel crosstalk describes the effect that another channel that is also necessary for the communication, such as the public channel or laser used for beacon system, strays into the quantum channel. It is also worth mentioning that additional light sources can be found on the QKD device's environment, e.g., the anticollision flashes of an aircraft.[8] Anthropogenic light, meaning light that is generated by human activities such as public illumination, building lighting, and vehicle headlights, is emitted into the atmosphere and arrives at the detector via scattering.

The amount of background light arriving at the detector depends on both the sources of background light as well as the propagation of the radiation through the atmosphere. The background photons are described in terms of the spectral radiance $I_\lambda(\vec{r}, \vec{\Omega}, t)$, where the spectral radiance can explicitly depend on the position $\vec{r}$, the observation direction $\vec{\Omega}$, and the time t. The value of the radiance field function $I_\lambda(\vec{r}, \vec{\Omega}, t)$ is determined using methods from radiative transfer theory. In the absence of interactions with the atmosphere, I_λ is governed by a continuity equation, familiar from hydro- and electrodynamics:

$$\frac{1}{c}\frac{\partial I_\lambda}{\partial t} + \vec{\Omega} \cdot \vec{\nabla} I_\lambda = 0. \tag{1}$$

The effects of interaction of photons with particles in the atmosphere are accounted for by adding appropriate terms to the right hand side of the equation. The dynamics of the radiance field coupled to the atmosphere are then determined by the radiative transfer equation:[9]

$$\frac{1}{c}\frac{\partial I_\lambda}{\partial t} + \vec{\Omega} \cdot \vec{\nabla} I_\lambda = -k_{\mathrm{ext},\lambda} I_\lambda + J_\lambda + \frac{k_{\mathrm{sca},\lambda}}{4\pi} \int_{4\pi} I_\lambda(\vec{\Omega}') \mathcal{P}_\lambda(\vec{\Omega}' \to \vec{\Omega}) d\vec{\Omega}'. \tag{2}$$

The terms on the right-hand side describe, in order, the absorption and out-scattering, emission, and in-scattering of photons. Absorption and scattering out of the detector's FOV are represented by the extinction coefficient $k_{\mathrm{ext},\lambda}$. Emission processes are described in terms of the source function J_λ. The integral term, modeling the scattering of photons into the detector's

FOV is determined by the scattering coefficient $k_{\mathrm{sca},\lambda}$ and the amplitude $\mathcal{P}_\lambda(\vec{\Omega}' \rightarrow \vec{\Omega})$ of a photon scattering from direction $\vec{\Omega}'$ to direction $\vec{\Omega}$. Note that k_{ext}, k_{sca}, J, and $\mathcal{P}$ are functions of $\vec{r}$, $\vec{\Omega}$, t, and λ. Therefore, the radiative transfer function takes direct and diffuse propagation into account.

Due to the presence of the scattering term and the number of parameters needed to model the atmosphere accurately, the radiative transfer equation is solved numerically. Popular numerical solvers such as LibRadtran[10] and MODTRAN[11] include parametrizations of molecule and aerosol distributions as well as absorption and scattering cross sections.

The simulated spectral radiance $I_\lambda\left[\frac{W}{m^2 msr}\right]$ can be converted to photon rate as

$$R_P = \frac{P \cdot \lambda}{\mathrm{h} \cdot \mathrm{c}}, \tag{3}$$

with the central wavelength λ, Planck's constant h, speed of light c, and the background light power

$$P = I_\lambda \cdot B_{\mathrm{eff}} \cdot \Omega_{\mathrm{FOV}} \cdot A_{\mathrm{rec}} \cdot \eta. \tag{4}$$

The transmittivity of the optical system is η. B_{eff} is the effective filter bandwidth describing the integral of the transmittivity of the filter as a function of wavelength. The receiver area is

$$A_{\mathrm{rec}} = \frac{\pi \cdot D_{\mathrm{R}}^2}{4}, \tag{5}$$

with the diameter of the receiver aperture D_{R}.

The solid angle FOV of the receiver Ω_{FOV} can be derived from the planar angle FOV θ_{FOV} and is approximately

$$\Omega_{\mathrm{FOV}} \approx \pi \cdot \theta_{\mathrm{FOV}}^2. \tag{6}$$

Furthermore, θ_{FOV} when coupling into an single mode fiber (SMF) can be described as

$$\theta_{\mathrm{FOV_{SMF}}} = \beta \cdot \frac{2}{\pi}\frac{\lambda}{D_{\mathrm{R}}}, \tag{7}$$

with $\beta = \beta_{\mathrm{opt}} = 1.12$ for unobstructed apertures.

Concluding that for SMF-coupled receivers the conversion from spectral radiance to background light power is

$$P_{\mathrm{SMF}} = I_\lambda \cdot B_{\mathrm{eff}} \cdot \beta^2 \cdot \lambda^2 \cdot \eta, \tag{8}$$

and therefore independent from D_{R}.[12]

3 Impact of Background Light on Free-Space QKD

An increase in the received background light will increase the QBER, which is in general described as

$$\mathrm{QBER} = \frac{\text{Erroneous clicks}}{\text{Total clicks}}. \tag{9}$$

The relation between QBER and background light depends on the specification of the QKD protocol and its physical implementation. Here, a decoy-state version of the BB84 protocol with polarization encoding of the qubits[13] is investigated further. In this protocol, also visualized in Fig. 1, Alice produces the quantum signal via attenuated laser pulses. More specific, Alice modulates the intensity and polarization of a laser pulse in order to prepare a quantum state. This quantum state has the polarization P and pulse intensity μ. The polarization $P \in \{\leftrightarrow, \updownarrow, \nearrow, \nwarrow\}$ can encode a qubit via the mapping $|\leftrightarrow\rangle \equiv |0\rangle, |\updownarrow\rangle \equiv |1\rangle$ and $|\nearrow\rangle \equiv \frac{1}{\sqrt{2}}(|0\rangle + |1\rangle), |\nwarrow\rangle \equiv \frac{1}{\sqrt{2}}(|0\rangle - |1\rangle)$. Three values for the signal intensity are considered here, which are $\mu \in \{\mu_0, \mu_1, \mu_2\}$, where μ_0 denotes the vacuum decoy pulse ($\mu_0 = 0$), μ_1 denotes the weak decoy pulse, and μ_2 denotes the signal pulse with $(0 < \mu_1 < \mu_2 < 1)$. Alice sends the quantum signal via a free space channel with end-to-end transmittivity η to Bob. Furthermore, an average amount of background light photons ν couple into the channel within the gating time Δt of the detector.

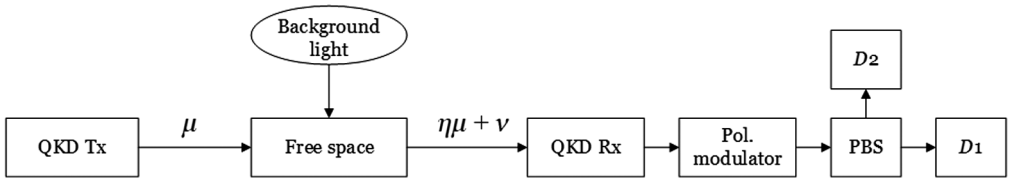

Fig. 1 A free-space decoy-state BB84 QKD setup with polarization encoding of qubits with the signal intensity of the laser pulse (μ), transmitting telescope (QKD Tx), attenuation (η), average number of background light photons (ν), receiver telescope (QKD Rx), polarizing beamsplitter (PBS), and detectors (D_1 and D_2).

In the following process, Bob will receive an average number of photons of $\tau = \eta\mu + \nu$. On Bob's side, the assumption is made that an active choice of measurement basis takes place.[14] The result is that two single-photon detectors are sufficient to perform the quantum state measurement in the BB84 protocol.

To calculate the QBER, the number of erroneous clicks and of total clicks needs to be derived for a realistic receiver model.[15] A single-photon detector is modeled as an ideal threshold detector preceded by a beam splitter with transmission η_{detector}. Dark counts are modeled as a stochastic process generating virtual photons that reach the ideal threshold detector at a rate equal to the estimated dark count rate (DCR) R_{D}. If τ is the average number of photons per pulse that reach a detector, the average number of virtual photons that reach the ideal threshold detector within a gating time Δt is then $\tau' = \tau\eta_{\text{detector}} + R_{\text{D}}\Delta t$. Since the virtual photons have, by assumption, a Poisson distribution and the ideal threshold detector clicks if there are $n \geq 1$ virtual photons, the probability of a click is $p_{\text{click}} = 1 - e^{-\tau'}$. The probability of the right (wrong) detector to click $p_{\checkmark}$ ($p_{\mathcal{X}}$) is then given as

$$\begin{cases} p_{\checkmark} = 1 - e^{-\tau_{\checkmark}\eta_{\text{detector}} - R_{\text{D}}\cdot\Delta t} \approx \tau_{\checkmark}\eta_{\text{detector}} + R_{\text{D}} \cdot \Delta t \\ p_{\mathcal{X}} = 1 - e^{-\tau_{\mathcal{X}}\eta_{\text{detector}} - R_{\text{D}}\cdot\Delta t} \approx \tau_{\mathcal{X}}\eta_{\text{detector}} + R_{\text{D}} \cdot \Delta t. \end{cases} \tag{10}$$

The approximation holds in the limit $\tau_{\checkmark}\eta_{\text{detector}} + R_{\text{D}}\Delta t \ll 1$. The light intensity expected at one detector ($\tau_{\checkmark}$ or $\tau_{\mathcal{X}}$) can be derived by taking the end-to-end transmittivity of the channel η, the mean photon number sent by Alice μ, and the average photon number of background light ν into account. Furthermore, misalignment between the state of preparation basis and the state of measurement basis (δ) can cause QBER as well. It follows that the pulse intensities at Bob's receiver in the two orthogonal states are given as

$$\begin{cases} p_{\checkmark}: & \tau_{\checkmark} \equiv \eta\mu\cos^2\delta + \frac{1}{2}\nu \\ p_{\mathcal{X}}: & \tau_{\mathcal{X}} \equiv \eta\mu\sin^2\delta + \frac{1}{2}\nu. \end{cases} \tag{11}$$

Three cases at the receiver can appear: (1) only the right detector clicks ($p_{\checkmark}(1 - p_{\mathcal{X}})$), (2) only the wrong detector clicks ($p_{\mathcal{X}}(1 - p_{\checkmark})$), and (3) both detector click and a random choice are made ($p_{\checkmark}p_{\mathcal{X}}$) to avoid so-called double-click attacks.[16]

This means the QBER is given as

$$\text{QBER} = \frac{p_{\mathcal{X}}(1 - p_{\checkmark}) + \frac{1}{2}p_{\checkmark}p_{\mathcal{X}}}{p_{\checkmark}(1 - p_{\mathcal{X}}) + p_{\mathcal{X}}(1 - p_{\checkmark}) + p_{\checkmark}p_{\mathcal{X}}} = \frac{p_{\mathcal{X}} - \frac{1}{2}p_{\checkmark}p_{\mathcal{X}}}{p_{\checkmark} + p_{\mathcal{X}} - p_{\checkmark}p_{\mathcal{X}}}. \tag{12}$$

It results that an optimization of the QBER in free-space QKD can be established by increasing the end-to-end transmittivity, increasing detector efficiency, decreasing DCR of the detector, and suppressing background light.

A QKD scenario is now illustrated to further show this dependency. Therefore, an effective filter bandwidth of 0.257 nm, a DCR of the detector of 2 kHz, a detector efficiency of 22%, a gating time of 1 ns, and a misalignment angle of the QKD setup δ of 5° and SMF-coupling is assumed. Figure 2 shows the dependency of end-to-end attenuation and QBER assuming different background radiation. The theoretical limit of a successful QKD is set to 11% corresponding to the ideal single-qubit version of the BB84 protocol.[17] The practical limit of 5% is taken from a reference experimental realization.[18] Figure 3 shows the dependency of background radiation and QBER assuming different end-to-end attenuation.

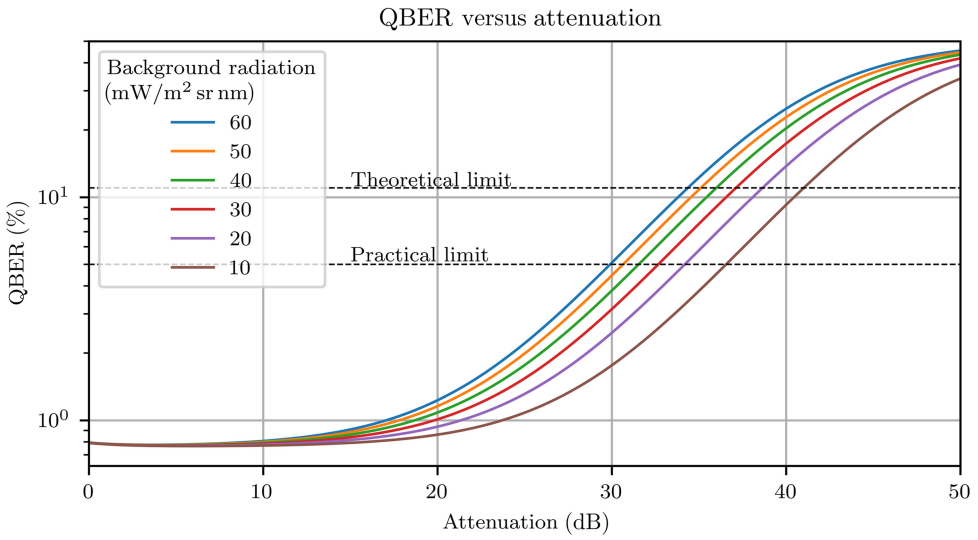

Fig. 2 Dependency of QBER and attenuation for different background light radiation of an exemplary QKD scenario with an effective filter bandwidth of 0.257 nm, a DCR of the detector of 2 kHz, a detector efficiency of 22%, a gating time of 1 ns, and a misalignment angle of the QKD setup δ of 5 deg and SMF-coupling.

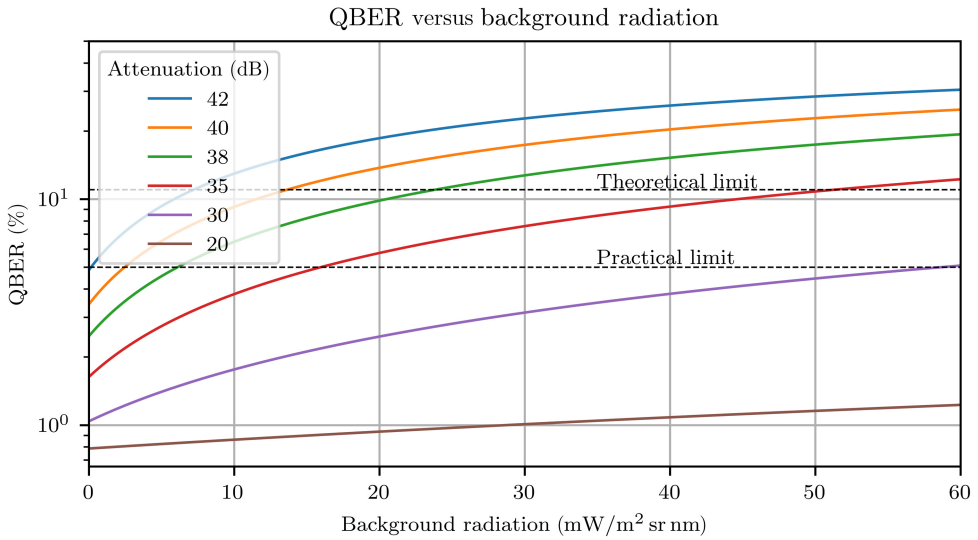

Fig. 3 Dependency of QBER and background light radiation for different attenuation of an exemplary QKD scenario with an effective filter bandwidth of 0.257 nm, a DCR of the detector of 2 kHz, a detector efficiency of 22%, a gating time of 1 ns, and a misalignment angle of the QKD setup δ of 5 deg and SMF-coupling.

The highest possible background light radiation is assumed to be 60 $\mathrm{mW/m^2srnm}$ regarding the simulation shown in Sec. 5.2. This means for the given example QKD is feasible for attenuation <30 dB in daylight. For higher attenuation, better filtering of the background light needs to be applied. In general, this plot can be produced to model the filtering parameters for a given setup.

4 Experimental Method to Investigate Background Light

To investigate background light experimentally, a fiber-coupled single-photon detector is used to detect the incoming photons. The single-photon sensitivity of the detector allows for measurement of short-term fluctuations in the amount of background light. In Fig. 4, the schematic of the measurement setup is described. A collimator couples in the background light, a bandpass filter in front of the collimator selects the wavelength to be observed. The single-photon detector

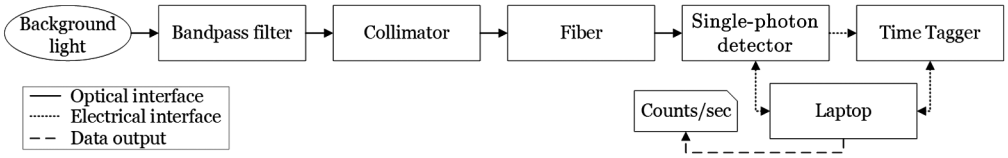

Fig. 4 Functional schematics of the background light measurement setup.

detects the incoming photons. The time tagger processes the clicks. A software on the laptop saves the count rate for subsequent data analysis. As a single-photon detector, the single photon avalanche diode (SPAD) infrared photon detection module (PDM-IR) micro photon devices (MPD) is used. As a time tagger, the Time Tagger Ultra (Swabian Instruments) is used. All used components, their characteristics, and the settings for the measurement are described in Table 2. The device itself must be shielded from stray light by placing the device in the shade and covering the whole setup with blackout fabric. To scan the sky in different azimuth and elevation angles, the collimator is mounted on a tripod.

The measured count rate $R_{\mathrm{P,meas}}$ of the detector is not the background light, which is actually present in front of the detector. The following parameters influence the measurable photons $R_{\mathrm{P,meas}}$:

- DCR of the detector R_{D}: detector clicks that are not caused by an incoming photon.
- Quantum efficiency of the detector η_{detector}: ratio between number of detection events to number of photons absorbed.
- Hold off time of the detector T_{holdoff}: time when detector is off after an avalanche breakthrough.

Therefore, the measured count rate $R_{\mathrm{P,meas}}$ needs to be rescaled to the real photon rate R_{P}. The R_{P} is the photon rate, which would be detectable, having an ideal detector meaning no DCR, 100% quantum efficiency and no hold off time. The conversion from $R_{\mathrm{P,meas}}$ to R_{P} is now shown. After every click, the detector is off for a given time T_{holdoff}. Having a look at the counts per second, the counts need to be corrected by the hold off time. The detector was activated for $(1\mathrm{s} - R_{\mathrm{P,meas}} \cdot T_{\mathrm{holdoff}})$ per second. Therefore, the percentage when the detector is activated is $1\ \mathrm{s}/(1\mathrm{s} - R_{\mathrm{P,meas}} \cdot T_{\mathrm{holdoff}})$. Subsequently, the arrival of background light photons can be modeled as a time-homogeneous Poisson process, hence the event count rate R_{E} is given as

$$R_E = \frac{R_{\mathrm{P,meas}}}{1 - R_{\mathrm{P,meas}} \cdot T_{\mathrm{holdoff}}}. \tag{13}$$

Table 2 Measurement setup of the background light measurement.

	Measurement device
Collimator	F230APC-1550, ThorLabs
	Alignment wavelength: 1550 nm
Bandpass filter	FB1550-12, Optical filter
	ThorLabs
	Wavelength: 1550 nm
	Full width at half maximum (FWHM): 12 nm
SPAD	PDM IR, MPD
	Hold off time: 100 μs
	DCR: 2000 Hz
	Quantum efficiency: 0.22
Time tagger	Time Tagger Ultra, Swabian Instruments

The same can be applied to convert the measurable DCR $R_{D,meas}$ to the real R_D. This takes into account that the detector is also not activated for $T_{holdoff}$ after every dark count

$$R_D = \frac{R_{D,meas}}{1 - R_{D,meas} \cdot T_{holdoff}}. \tag{14}$$

The real photon rate R_P can be calculated by subtracting R_D from R_E and dividing by the quantum efficiency of the detector $\eta_{detector}$

$$R_P = \frac{R_E - R_D}{\eta_{detector}}. \tag{15}$$

5 Result of the Background Light Measurement

5.1 Background Light Measurement by Scanning Clear Sky

The background light measurement was conducted at the rooftop of the Institute's building in Oberpfaffenhofen (Germany) with an elevation range from 10 deg to 80 deg in 10 deg steps. Each step held a measurement duration of 180 s. Azimuth angles were selected to be 30 deg, 60 deg, and 350 deg. The measurement was performed from 12 pm to 3 pm on April 21, 2022. The sky was clear from clouds except for some clouds at low elevation. Figure 5 shows the photon rate traces that are already calibrated by means of detector performance metrics. Therefore, the photon rate represents the photons in front of the detector. The conversion method from count rate to photon rate is described in Sec. 4.

5.2 Comparison of Experimental and Simulated Background Light Data

Using LibRadtran predictions for different sun elevation angles, sky radiance maps can be plotted as can be seen in Fig. 6. To establish comprehensible simulation data, the position of the sun at each data point is calculated using LibRadtran's zenith tool. The solar azimuth angle was in the range 161 deg to 180 deg for the measurements at 0 deg azimuth, and 183 deg to 195 deg and 202 deg to 224 deg for the measurements at 30 deg azimuth and at 60 deg azimuth, respectively.

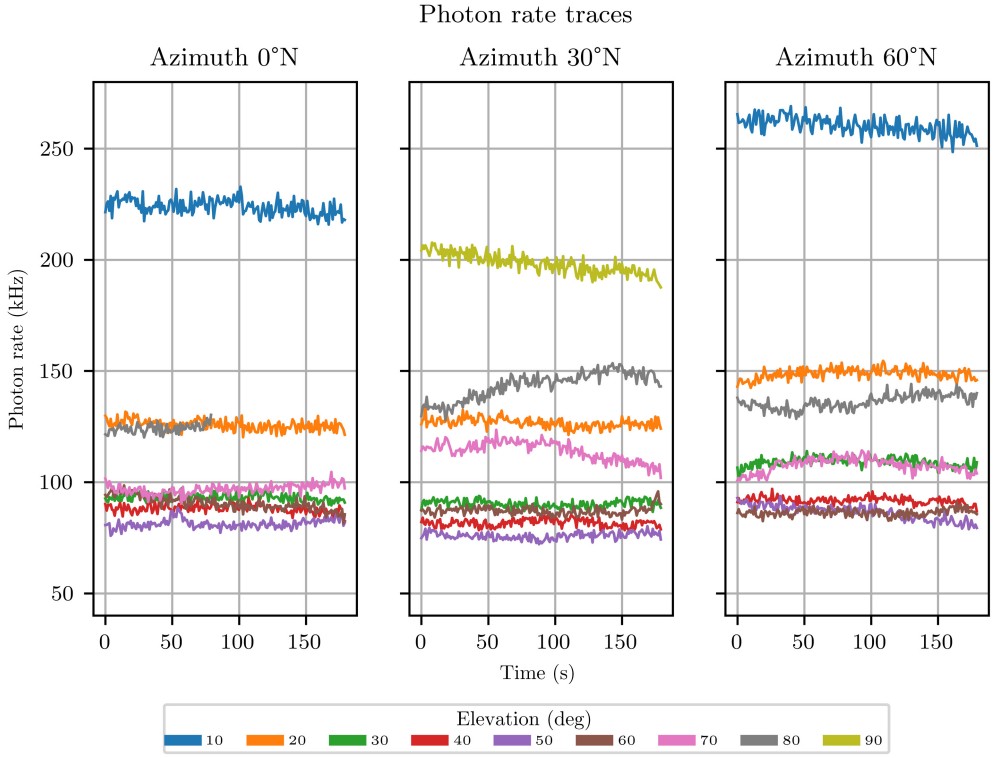

Fig. 5 Photon rate trace in daylight for different azimuth and elevation angles with the setup in Table 2, effective bandwidth $B_{eff} = 7.8$ nm and transmittivity $\eta = 0.51$.

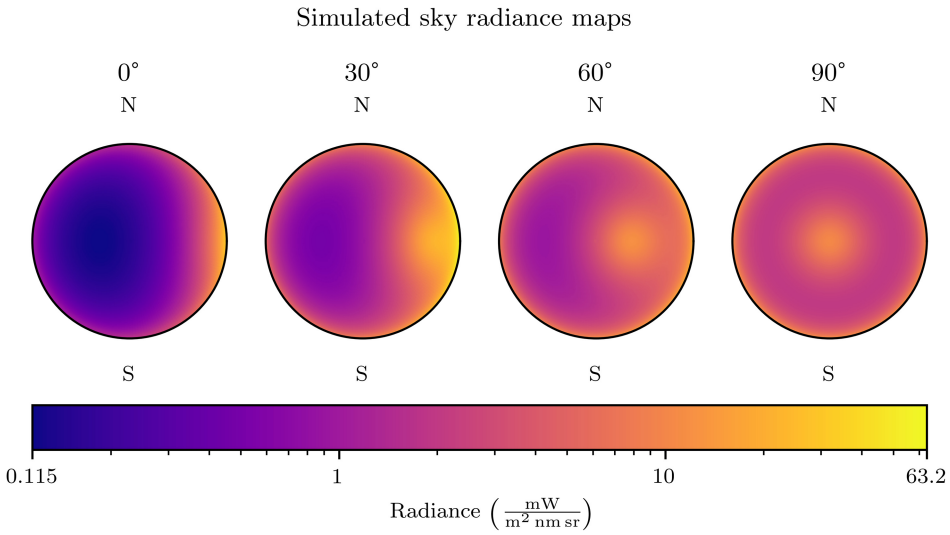

Fig. 6 Sky radiance map simulated with LibRadtran for the location Oberpfaffenhofen, Germany, and the spectral radiance at 1550 nm using the sun's spectrum[7] and LibRadtran's default aerosol model.[19]

The solar elevation angle changed from 54 deg during the first measurement (performed at around 12:30) to 46 deg during the last (performed at around 15:00). Given the location of the measurement setup (Oberpfaffenhofen, Germany), the collimator viewing direction and the corresponding solar position, the spectral radiance at 1550 nm is calculated with LibRadtran using the sun's spectrum[7] and the implemented aerosol model by Shettle.[19] The aerosol model is used in default setting meaning a rural type aerosol in the boundary layer, background aerosol above 2 km, spring–summer conditions, a visibility of 30 km and an albedo of 0.15.[19,20] The visibility and the albedo are fitted to the experimental results and are within the reasonable regime. Then the spectral radiance is converted to the photon rate using the method described in Sec. 2 and $B_{\mathrm{eff}} = 7.8$ nm and $\eta = 0.51$.

6 Interpretation of the Background Light Measurement

The photon rate is stable and showing no rapid fluctuations. As an example, the mean accounts 87.1 kHz, the peak-to-peak value 12.6 kHz, and the standard deviation 1.8 kHz for the measurement at 60.6 deg elevation and 39 deg azimuth.

The comparison of measured and simulated photon rates is shown in Fig. 7. It shows the mean photon rates in three plots corresponding to the three azimuth directions. The measurement and simulation show a high degree of agreement in an elevation range between 10 deg and 90 deg. This indicates that the simulation tool delivers accurate results according to the current assumptions of a clear sky applied by the simulation tool. At the same time, these clear-sky assumptions limit the accuracy in real-world applications. Weather influences are difficult to implement in a simulation.

This shows that for predictions of background light in a scenario with clear sky and in a rural environment, simulation tools are sufficient. For air-to-ground scenarios, the mobile node can be in front of clouds. This leads to an increase of background light, which cannot be simulated at the moment. Comprehensive measurements and analysis of the sky are necessary to determine best- and worst-case background light values for different weather conditions and time of the day and year. For satellite-to-ground scenarios, the channel must not be blocked. Therefore, simulated background light can represent a good estimation of the expected background light during the day. Partly clouded sky cannot be simulated but can be investigated with this setup. Further missing investigations to validate the simulated background light at night are to analyze the effects of the Moon, stars, and planets as well as anthropogenic light. Therefore, a setup as presented in Sec. 4 can be used to carry out a site inspection beforehand. Furthermore, channel crosstalk needs to be considered for each scenario individually.

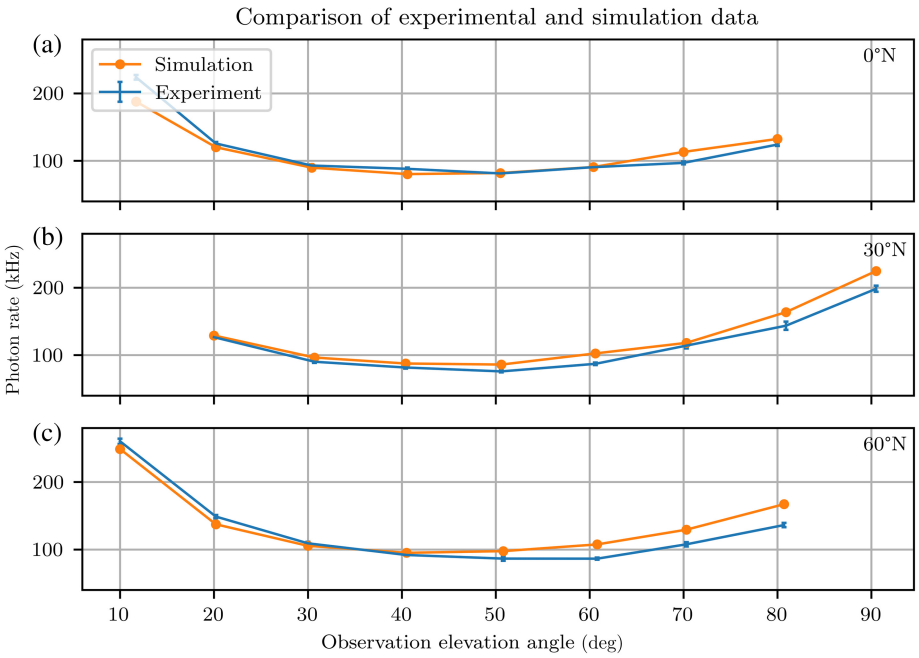

Fig. 7 Comparison of the experimental and simulated photon rate using the measurement setup in Table 2, effective bandwidth $B_{\text{eff}} = 7.8$ nm and transmittivity $\eta = 0.51$ with the average position of the sun during the measurement period for the 0 deg azimuth measurement (a) az. 171 deg, el. 53 deg, for the 30 deg azimuth measurement (b) az. 189 deg, el. 54 deg, and for the 60 deg azimuth measurement (c) az. 210 ded, el. 51 deg.

7 Conclusion

Since the transmission channel for satellite-based QKD is in free-space, background light is coupling in. The received background light leads to false detection events at the receiver and thus to an increase in QBER. The exact dependency between QBER and background light depends on the selected protocol. Above a certain threshold, the QBER can no longer be corrected by postprocessing and QKD protocol has to abort the secure key generation. The background light can be counteracted with the help of temporal, spectral, and spatial filters. To define the requirements for background light reduction techniques, the expected background light must be known. The main source of background light during the day is the diffuse impact of the Sun. The propagation of the light through space till the receiver is described by the radiative transfer equation, which can be solved by simulation tools such as LibRadtran and MODTRAN. These simulation tools are limited to the assumption of a cloud-free sky and rural environment. An experiment scanning a sky shows a high correlation between the results and the simulation when the sky is cloud-free, which verifies the simulation tool. Nevertheless, cloudless skies are mostly rare and therefore the current forecast of simulation tools is not entirely sufficient to provide accurate information. Clouds can not only block the channel completely but can also cause an increased sky brightness, which scatters into the channel. This concludes that an experimental investigation is necessary at the moment. To derive more precise action recommendations for noise suppression, more measurement data need to be collected at different seasons and weather conditions.

Code and Data Availability

The data that support the findings of this study are available from the corresponding author, Stefanie Häusler, upon reasonable request.

Acknowledgments

The project on which this report is based was funded by the German Federal Ministry of Education and Research (Grant No. 16KIS1265). The authors are responsible for the content of this publication.

References

1. M. Er-long et al., "Background noise of satellite-to-ground quantum key distribution," *New J. Phys.* **7**, 215 (2005).
2. M. T. Gruneisen et al., "Modeling daytime sky access for a satellite quantum key distribution downlink," *Opt. Express* **23**, 23924 (2015).
3. A. Tomaello et al., "Link budget and background noise for satellite quantum key distribution," *Adv. Space Res.* **47**, 802–810 (2011).
4. C. Bonato et al., "Feasibility of satellite quantum key distribution," *New J. Phys.* **11**, 045017 (2009).
5. M. T. Gruneisen et al., "Adaptive spatial filtering for daytime satellite quantum key distribution," *Proc. SPIE* **9254**, 925404 (2014).
6. G. W. Petty, *A First Course in Atmospheric Radiation*, Sundog Publishing (2006).
7. R. L. Kurucz, "Synthetic infrared spectra," in *Symp.-Int. Astron. Union*, Cambridge University Press, Vol. **154**, pp. 523–531 (1994).
8. S. Nauerth et al., "Air to ground quantum key distribution," *Proc. SPIE* **8518**, 85180D (2012).
9. W. Zdunkowski, T. Trautmann, and A. Bott, *Radiation in the Atmosphere: A Course in Theoretical Meteorology*, Cambridge University Press (2007).
10. C. Emde et al., "The LibRadtran software package for radiative transfer calculations (version 2.0.1)," *Geosci. Model Dev.* **9**, 1647–1672 (2016).
11. A. Berk et al., "MODTRAN 6: a major upgrade of the MODTRAN radiative transfer code," in *6th Workshop on Hyperspectral Image and Signal Process.: Evol. in Remote Sens. (WHISPERS)*, IEEE, pp. 3–4 (2014).
12. A. Scriminich et al., "Optimal design and performance evaluation of free-space quantum key distribution systems," *Quantum Sci. Technol.* **7**, 045029 (2022).
13. H.-K. Lo, X. Ma, and K. Chen, "Decoy state quantum key distribution," *Phys. Rev. Lett.* **94**, 230504 (2005).
14. N. Gisin et al., "Quantum cryptography," *Rev. Mod. Phys.* **74**, 145–195 (2002).
15. P. P. Rohde and T. C. Ralph, "Modelling photo-detectors in quantum optics," *J. Mod. Opt.* **53**(11), 1589–1603 (2006).
16. D. Gottesman et al., "Security of quantum key distribution with imperfect devices," in *Proc. Int. Symp. on Inf. Theory (ISIT)*, IEEE, p. 136 (2004).
17. S. Pirandola et al., "Advances in quantum cryptography," *Adv. Opt. Photonics* **12**, 1012–1236 (2020).
18. I. D. Marco et al., "Real-time operation of a multi-rate, multi-protocol quantum key distribution transmitter," *Optica* **8**, 911–915 (2021).
19. E. P. Shettle, "Models of aerosols, clouds, and precipitation for atmospheric propagation studies," in *AGARD Atmos. Propag. in the UV, Visible, IR, and MM-Wave Region and Related Syst. Aspects* (1990).
20. B. Mayer et al., "LibRadtran user's guide," p. 48 (2012).

Stefanie Häusler received her bachelor's degree in engineering physics and her master's degree in applied research in engineering science from Deggendorf Institute of Technology. As a student, she gained experience in the field of Satellite Laser Ranging at Geodetic Observatory Wettzell (2018–2021). Since 2021, she has been at the German Aerospace Center (DLR), Institute of Communications and Navigation in the Quantum Communication Group led by Florian Moll, focusing on Optical Ground Stations for satellite-based Quantum Key Distribution.

Davide Orsucci received his master's degree in theoretical physics from the University of Pisa and Scuola Normale Superiore in 2014 and his PhD in quantum computation under Prof. Hans Briegel, Innsbruck, in 2018. After a post-doc on quantum optics in Basel in 2019, since 2020, he has been at the German Aerospace Center (DLR) in the Quantum Communication Group led by Florian Moll, working on Quantum Key Distribution, free-space optical communication, atmospheric channel modeling and quantum repeater architectures.

Leonard Vollmann received his bachelor's degree in physics from Ludwig-Maximilians-University (LMU) Munich, in 2021. Since 2021, he has been enrolled in the graduate course "Theoretical and Mathematical Physics" at LMU Munich and Technical University of Munich. Since 2021, he has been a student at the German Aerospace Center (DLR), Institute of Communications and Navigation in the Quantum Communication Group led by Florian Moll.

Eltimir Peev received his master's degree in engineering physics with specialization in lasers and optics from the University of Oldenburg in 2014. After spending several years as a researcher in the field of nonlinear optical microscopy and spectroscopy, he joined the Quantum Communications Group at the German Aerospace Center (DLR) (2020–2023). Currently, he is a consultant for projects involving free space optics, opto-electronics, optical instrumentation, and systems engineering.

Florian Moll received his Dipl. Ing degree in electrical engineering from Jena University of Applied Sciences in 2006 and his MSc degree in electrical engineering from Technische Universität München (TUM) in 2009. He has been a member of the German Aerospace Centre (DLR), Institute of Communications and Navigation since then. His work area is free-space optical quantum communications and telecommunications for aircraft and satellites. His main research interests are the connections between LEO and GEO satellites, aircraft, and ground stations; characterization of the propagation channel; and optics design. He has been involved in several research projects as a project leader and a team member, dealing with classical and quantum communications. Since 2020, he has been the head of the research group in Quantum Communications Systems.